

Druckfreigabe/approval for printing	
Without corrections/ ohne Korrekturen	<input type="checkbox"/>
After corrections/ nach Ausführung der Korrekturen	<input type="checkbox"/>
Date/Datum:	.....
Signature/Zeichen:	.....

## 17 Bifunctional Surfaces

*Wolfgang Knoll, Amal Kasry, and Jakub Dostalek*

### 17.1 Introduction

The general topic of biofunctional interfacial architectures has seen in recent years a remarkable growth of interest and research activities [1]. On the one hand, this is mostly triggered by the general belief that the construction of an interactive interface between the “living” world of biomolecules, cells, tissue, or whole organisms and the (organic or inorganic) materials world of technical devices like implants, medical parts, or sensors requires the proper design and construction and the detailed structural and, in particular, functional characterization and control of this organism–machine interface [2]. We are still at the very beginning of obtaining a better understanding of what is needed to make an organism tolerate implants, to guarantee the bidirectional communication between microelectronic devices and living tissue, or to simply construct an interactive biocompatibility of surfaces in general.

Generally, the strategies for the synthesis of supramolecular interfacial architectures (cf. Figure 17.1), designed for a particular functional performance, include simple self-assembled monolayers (SAMs), as well as (polymer) brushes, dendrimer layers, hydrogels, or (interpenetrating) networks [1]. Specific attention in the corresponding literature is given to the fabrication and assembly of interfacial layers made from peptides, proteins, or saccharides, and to the design and characterization of supported or tethered lipid bilayer membranes. And finally, the control of the architecture and functional performance of whole cells and cell assemblies with surfaces has attracted special attention because of its importance for the design of sustainable implant surfaces, in tissue engineering, or for regenerative medicine applications.

On the other hand, already the relatively simple interface between a technical transducer used in a biosensor format and the analyte solution of interest constitutes a challenge for the supramolecularly controlled assembly of the interfacial architecture. In addition to the need for optimizing the selective interaction

Color Fig.: 17.1

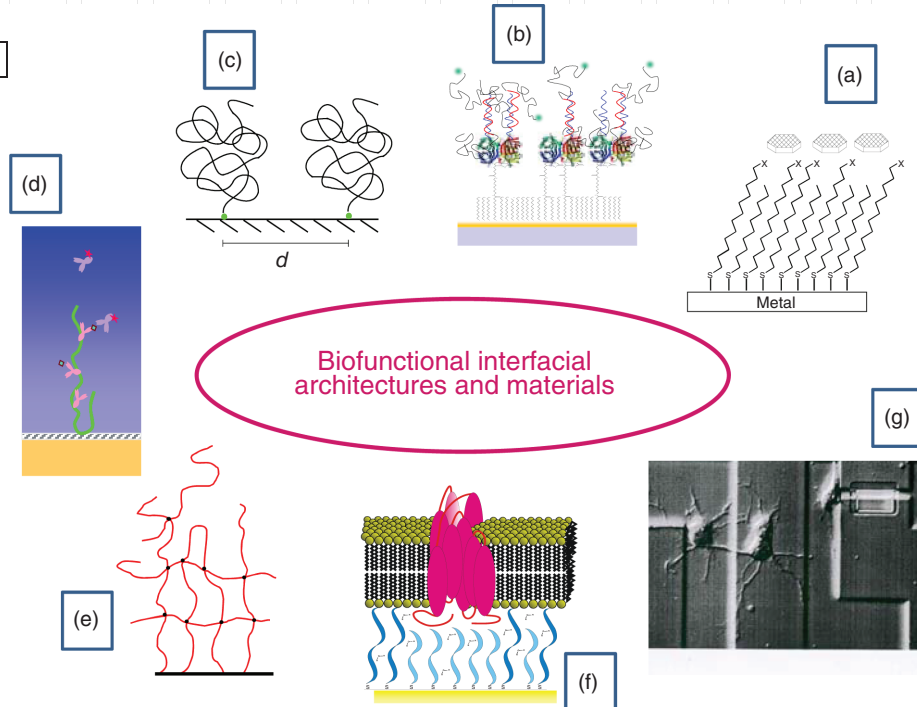


**Figure 17.1** Various examples of biofunctional interfacial architectures: (a) self-assembled monolayer with a particular functional chemical moiety,  $x$ , that initiates the nucleation and growth on inorganic crystals; (b) supramolecularly controlled interfacial multilayer architecture, involving a self-assembled monolayer of biotin-functionalized thiol derivatives, a layer of bound streptavidin, with associated biotinylated oligonucleotide single strands, used as capture probes for the surface hybridization

of fluorophore-labeled PCR amplicons; (c) polymer brush, that is, a monolayer of end-grafted linear polymer chains; (d) such a brush used as binding matrix for antibodies, recognized by another fluorophore-labeled antibody; (e) simplified schematic sketch of a surface-grafted hydrogel; (f) tethered bimolecular lipid membrane with a reconstituted membrane protein; and (g) single primary neurons growing (with dendrite and axon formation) on a microelectronic chip.

between the specific binding sites at the sensor surface and the analyte from solution, one of the major tasks for the proper design of the interfacial biofunctional architecture, actually, is the minimization of the nonspecific binding of other biomolecules from a physiological solution or from body liquids (see Figure 17.2). Typically, these species are by far in excess, and even weak unspecific interaction can generate significant interfacial signal interfering with that originating from the specifically bound biomolecule of interest [3].

As an example, the gene chip is a well-established analytical platform for the detection of oligonucleotides, polymerase chain reaction (PCR) amplicons, generic DNA (fragments), and so on, used already for a variety of biological and

Color Fig.: 17.2

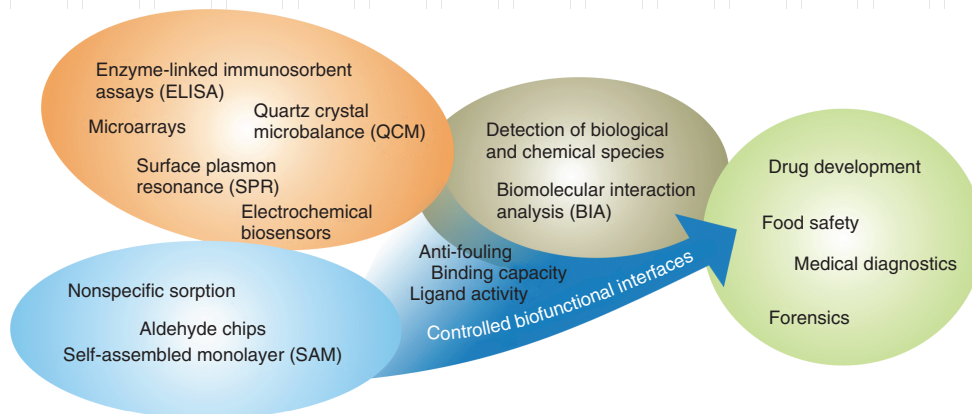


**Figure 17.2** Interfacial architectures as enabling technology for detection and interaction analysis of chemical and biological species by using heterogeneous assays.

medical applications. Still, many questions remain to be solved; associated, for example, with the fact that DNA intrinsically is a highly charged polyelectrolyte system. Other than in a dilute bulk solution, at an interface, this feature can cause all kinds of problems related, for example, to the coulombic interaction of the surface-attached capture probes with the analyte target strands binding from solution, or the possible crosstalk between neighboring hybridization sites, to mention but a few [4].

Not quite at the same level of maturity, however, already beyond a purely experimental stage, are arrays that detect various kinds of proteins, with applications ranging from monitoring expression levels of proteins to helping in cancer diagnostics and other disease detection [5]. Here, the practical problems are still much more serious than in the case of the gene chip, but first commercial products appear on the market.

And finally, a membrane chip does not exist at all. For many years, despite some interesting general scientific papers that appeared in the literature [6, 7], no report about the successful introduction of a prototype or a real product has appeared so far. But the experimental platform of supported or tethered lipid bilayer membrane is much more general [8] and allows for a broad portfolio of potential application such as binding studies in drug development addressing membrane-integral receptors. Moreover, it holds potential for the elucidation of membrane-associated pathogenic processes, like the amyloid plaque formation in the development of Alzheimer's disease [9], allows for its use as a "phantom cell" for a detailed evaluation of the essential processes underlying cell-cell contact, for example, in cancer development, for general tissue engineering purposes, or for the development of strategies to overcome current concerns for classical antibiotics which find more and more bacterial

Druckfreigabe/approval for printing	
Without corrections/ ohne Korrekturen	<input type="checkbox"/>
Trim Size: 170mm x 244mm	
After corrections/ nach Ausführung der Korrekturen	<input type="checkbox"/>
Date/Datum:	.....
Signature/Zeichen:	.....

#### 4 | 17 *Biofunctional Surfaces*

strains resistant to the traditionally applied antibiotic drugs (or even drug cocktails).

In this short chapter, we will summarize some of our efforts in the design, the assembly, the structural and functional characterization, and the sensor application of interfacial layers with molecularly or supramolecularly controlled architectures on solid substrates [10]. We first present a few considerations for the detection of DNA amplicons hybridizing from solution to surface-grafted capture oligonucleotide strands. Then we turn to polymer brushes, functionalized by mouse antibodies. These can be recognized by rat anti-mouse antibodies (RaM-ABs) carrying a chromophore that can be very sensitively detected by surface plasmon fluorescence spectroscopy (SPFS). And finally, we present the concept of the tethered bimolecular lipid membrane (t-BLM) as a novel surface-grafted model membrane system that allows for a variety of studies of and with these artificial membranes. Particular emphasis in these examples will be put on the correlation between the functional requirements for any of these interfacial layers, and their molecular and supramolecular organization and structural design needed to meet these targets.

##### 17.2 Supramolecularly Controlled Oligonucleotide Architectures for PCR (DNA Amplicon) Biosensing

The protocol for the detection of specific PCR target amplicons via a surface recognition and binding (hybridization) reaction by/to capture probe strands immobilized to the transducer surface needs to take into account the fact that PCR products are typically double-stranded DNA sequences of 100–250 bp in length. This requires that the double strands must be first converted to single strands and re-hybridization in solution must be prevented in order to allow for an efficient binding of the sense (single) strand to the surface capture probe for detection. The protocol that we developed to specifically bind and monitor the sense strand, in particular, with a significant discrimination between strands of different mismatches (detection of single nucleotide polymorphism, SNP) starts with the double strands as obtained by regular PCR (Figure 17.3a) [11]. By heating the solution to a temperature above the melting temperature, we achieve a separation of the double strand into two individual single strands and prevent efficient, that is, in particular, fast re-hybridization by quenching the solution to a low-salt buffer (Figure 17.3b). The low ionic strength of this buffer switches on the electrostatic repulsion of the highly charged single strands, thus keeping them apart (Figure 17.3c).

An uncharged DNA mimic, a 15mer peptide nucleic acid (PNA) oligonucleotide of a particular sequence (Figure 17.3e) complementary to a 15mer sequence in the middle of the single-stranded sense amplicon, offers means for the surface hybridization that is by no means hindered by coulombic interaction and is ionic strength independent. Hence, this surface reaction can well occur even under

Color Fig.: 17.3

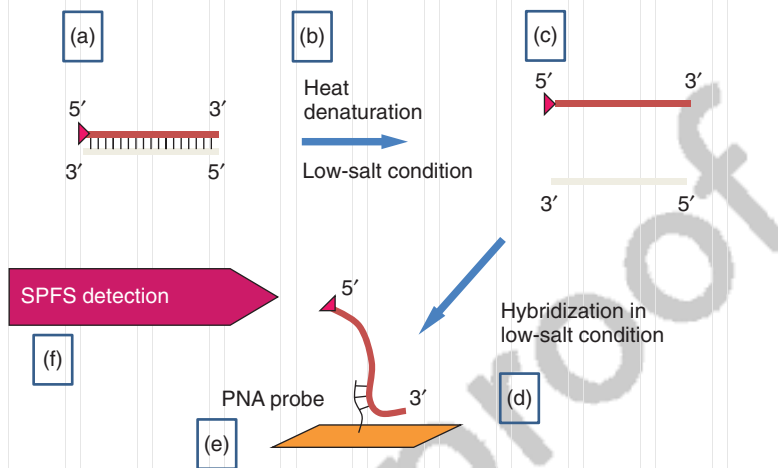


**Figure 17.3** Sequence of steps in a protocol developed for the detection of PCR amplicons: starting with the typically double-stranded PCR products of interest (a), they are first heat-denatured (b), and then quenched into a low-ionic strength buffer (c) that prevents a (rapid) re-hybridization in solution. This allows then for the individual single strand to bind to the surface-grafted

complementary capture strand made from synthetic peptide nucleic acids (PNAs) (e) that are uncharged. This process, hence, is independent of the low ionic strength (d). The amplicons carry a chromophore that allows for an extremely sensitive detection by surface-plasmon fluorescence spectroscopy (ff), cf. also text).

conditions that prevent bulk (re-)hybridization (Figure 17.3d). With the analyte strand now being bound to the transducer, various biosensors can be applied for the detection of the surface coverage as a function of time for the quantitative evaluation of  $k_{\text{on}}$  and  $k_{\text{off}}$  rate constants or as a function of the bulk concentration,  $c_0$ , for the determination of affinity constants ( $K_A$  and  $K_d$ ). We should point out that the surface architecture of the capture layer is based on a generic streptavidin coupling concept, hence offers a maximum surface coverage of  $2.5 \times 10^{12}$  binding sites  $\text{cm}^{-2}$ . This minimizes the crosstalk between neighboring sites upon binding (hybridization) of the highly charged DNA amplicons and allows for a near pure Langmuir adsorption process (at least at ionic strengths of typical hybridization buffers).

In next sections, we describe our observations of molecular interactions on a metallic surface with controlled interfacial architectures by using combined surface plasmon resonance (SPR) and SPFS. As shown in Figure 17.4, these methods are implemented by using a Kretschmann configuration of attenuated total reflection method. Briefly, a laser beam was coupled to an optical prism with optically matched sensor chip that carried a thin metal film and investigated surface architecture on the top. To the sensor chip, a flow cell was clamped in order to flow analyzed liquid samples with dissolved analytes of interest. The laser beam was resonantly coupled to surface plasmons that probed the binding of target species on the biosensor surface. This interaction was observed through

Color Fig.: 17.4

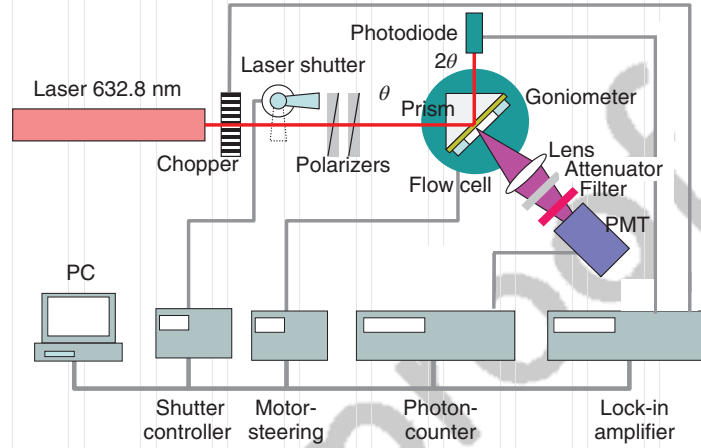


**Figure 17.4** Optical system used for the combined surface plasmon resonance (SPR) and surface plasmon-enhanced fluorescence spectroscopy (SPFS) studies of molecular interactions at supramolecularly controlled interfacial architectures.

Color Fig.: 17.5

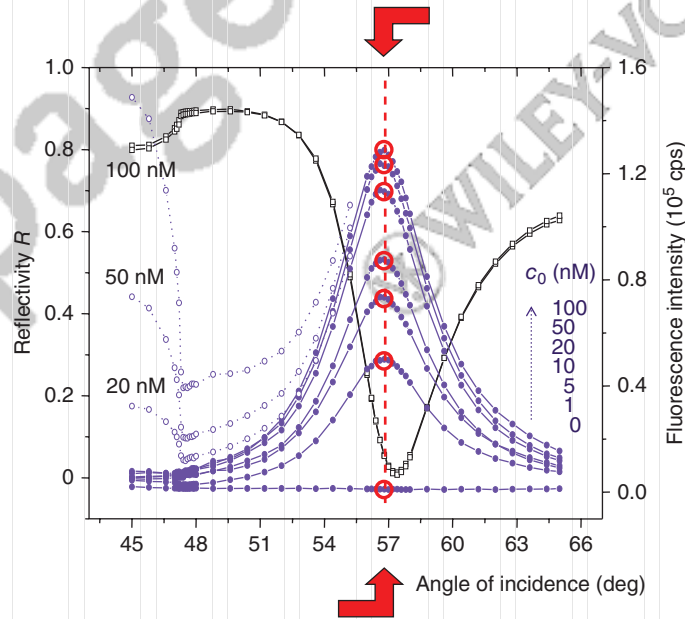


**Figure 17.5** Angular reflectivity (black) and fluorescence (blue) scans taken before the hybridization, that is, in pure buffer, and after running the hybridization reactions to completion in various concentrations (as indicated) of the single-stranded amplicons

(open symbols and dotted curve) and after exchanging the amplicon solution against pure buffer (full symbols and full curve). Note the saturation behavior of the fluorescence intensity as one increases the bulk intensity over two orders of magnitude.

Druckfreigabe/approval for printing	
Without corrections/ ohne Korrekturen	<input type="checkbox"/>
After corrections/ nach Ausführung der Korrekturen	<input type="checkbox"/>
Date/Datum:	.....
Signature/Zeichen:	.....

## 17.2 Supramolecularly Controlled Oligonucleotide Architectures | 7

the induced refractive index changes that are accompanied with detuning of SPR or by using additional fluorophore labels that, when adhered to the surface, were excited via the enhanced field intensity of surface plasmons and emitted fluorescence light was recorded by a photomultiplier. The angle of incidence  $\theta$  of the laser beam that was totally internally reflected at the sensor surface was controlled with a rotation stage in order to tune the coupling strength to surface plasmons.

For the further described DNA hybridization experiments, a fluorescence label was introduced at the 5' end of the sense strand by using an appropriately labeled primer sequence (the red triangle at the 5' end of the sense strand in Figure 17.3). The recorded series of SPR reflectivity scans (open black circles and the full black curves) and fluorescence intensity angular spectra recorded after the completion of the hybridization reaction are shown in Figure 17.5. The angular fluorescence spectra were measured before rinsing the cuvette, that is, exchanging the amplicon solution against pure buffer (as the open blue symbols with the broken curve, cf. Figure 17.5), as well as after rinsing of the flow cell, that is, after removing any bulk DNA strands (full blue symbols and full blue curve in Figure 17.5). Since  $k_{\text{off}}$  is so low for this experiment (as derived from the kinetic measurements, not shown here), there is sufficient time to take these angular recordings without losing any DNA strands from the surface by a dissociation process back into the bulk liquid buffer. The different measurements shown in Figure 17.5 are taken at different bulk amplicon concentrations, as indicated, varied between 0 and 100 nM [12] and key observations are summarized in Table 17.1.

Calibration curve can be established from these data by plotting the fluorescence intensity measured at a fixed angle of observation ( $\theta = 57$  deg in our case; cf. the red arrows, open circles and broken line in Figure 17.5) as a function of the bulk concentration,  $c_0$  (Figure 17.6). By fitting the experimental data to a Langmuir adsorption model, one obtains an affinity value of  $K_A = 3.7 \times 10^8 \text{ M}^{-1}$ , corresponding to a half-saturation concentration of  $K_d = 2.7 \text{ nM}$ . That is, at this value of the bulk concentration, half of the binding sites (the surface bound capture probes) are occupied. This translates to a surface coverage of  $\sigma = 1 \times 10^{12} \text{ amplicons cm}^{-2}$  which is too low to be detected label-free, however easily seen with a very comfortable  $S/N$  ratio by SPFS.

With this sensitivity, one can then look into the limit of detection, LOD. This is done in the purely mass transfer-limited regime, that is, at extremely low analyte bulk concentration where – upon switching from pure buffer running through the flow cell to an amplicon solution of the desired (low) concentration – the mere diffusion of the analyte across the unstirred layer leads to a linear increase of the fluorescence intensity. This is shown in Figure 17.7a for a series of bulk concentrations ranging from 1 to 100 pM. After monitoring each binding process for a certain time, the sensor surface was regenerated by rinsing NaOH through the flow cell, resulting in a rather abrupt dissociation of the hybridized amplicons. By recording the increase for the different concentrations, fitting the data to a linear increase of the fluorescence intensity with time, and plotting the slope of

Druckfreigabe/approval for printing	
Without corrections/ ohne Korrekturen	<input type="checkbox"/>
After corrections/ nach Ausführung der Korrekturen	<input type="checkbox"/>
Date/Datum:	.....
Signature/Zeichen:	.....

8 | 17 *Biofunctional Surfaces*

**Table 17.1** Key observations of SPFS/SPR investigation of amplicon hybridization.

(i)	All reflectivity curves irrespective of the solution concentration at which they were taken are indistinguishable. This means that the low surface density that can be achieved with this capture probe architecture does not lead to a significant change in the optical properties of interfacial architecture upon hybridization – even at 100% hybridization efficiency. Hence, a label-free detection of this surface reaction is not possible.
(ii)	The fluorescence intensities measured below the critical angle of total internal reflection at about $\theta = 47.3$ deg originates from the chromophores of the labeled PCR amplicons in solution excited by the (little) laser light intensity (reflectivity 80%, cf. Figure 17.5) that is transmitted through the Au film used in the Kretschmann configuration of the SPR setup as the base substrate. This intensity scales linearly with the bulk concentration (measured over the two orders of magnitude in concentration, not shown here) and can be used (after proper calibration) for an independent determination of the analyte bulk solution concentration.
(iii)	This fluorescence is completely gone after rinsing the cell with pure buffer solution washing out all bulk amplicons (cf. the full blue curves in Figure 17.5).
(iv)	What is left is the fluorescence light emitted from the chromophores of the surface-bound DNA strands upon excitation by the surface plasmon mode. By varying the angle of incidence, the resonant excitation of this surface light is turned on and off again as one sweeps through the resonance angle. Note, however, that the maximum fluorescence intensity does not occur at the angle of the lowest reflectivity but slightly before that, following the excitation profile of the surface mode. The reflectivity curve is the result of interference between the surface plasmon mode and the directly reflected light, with a (nearly) complete destructive interference at the minimum angle of the reflectivity which occurs at a slightly higher angle than that of the maximum plasmon mode excitation.
(v)	The fluorescence intensity originating from the surface-associated DNA strands measured after the completion of the hybridization reaction at different bulk amplicon concentrations (and after rinsing) shows – other than the fluorescence intensity from the bulk solution – a clear saturation behavior.

these lines as a function of the bulk concentration (cf. Figure 17.7b), one obtains a calibration curve that scales linearly with the bulk concentration. That is, with a 10-fold increase of the bulk concentration, the speed of fluorescence increase, the slope of this increase increases by a factor of 10 – as it should be for a mass transfer-limited diffusion across the unstirred layer. The calibration curve intersects with the noise level of bulk fluorescence baseline of the setup (described as three times standard deviation) at a concentration that defines the LOD for this system. In our case of DNA amplicon detection by SPFS, this amounts to an LOD = 100 fM.

17.3 Polymer Brushes for the Ultrasensitive Detection of Antibodies | 9

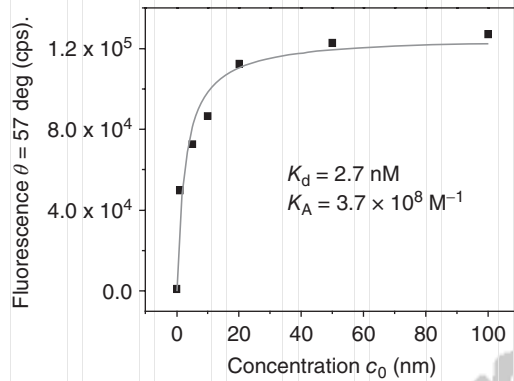


**Figure 17.6** Langmuir adsorption isotherm for the binding of the chromophore-labeled amplicon by plotting the peak fluorescence intensities taken at a fixed angle of observation  $\theta = 57$  deg (cf. also the red arrows and dashed line in Figure 17.5) as a function of the corresponding bulk solution. The symbols are the experimental data points (taken from Figure 17.5) and the full curve is a Langmuir fit to the data resulting in the affinity constant  $K_A = 3.7 \times 10^8 \text{ M}^{-1}$  (corresponding to a half-saturation concentration of  $K_d = 2.7 \text{ nM}$ ).

**17.3 Polymer Brushes for the Ultrasensitive Detection of Antibodies**

The optimized interfacial architecture for DNA amplicon detection is best realized by a planar 2D design because the monitored affinity reaction between the surface-immobilized capture probe strand (even if working with uncharged PNA oligonucleotide strands) and the DNA amplicon from solution leads to a highly charged interfacial polyelectrolyte brush. The resulting thickness of this analyte brush of a few nanometer is typically significantly thinner than the evanescent tail of the probing surface plasmon mode, which in the case of a classical SPR setup extends into the analyte solution some 10–100 nm, depending on the used metal and the employed laser wavelength (e.g., for Ag and a HeNe laser operated at  $\lambda = 632.8 \text{ nm}$ , the  $1/e$  decay of the evanescent field amplitude is  $L_p \sim 170 \text{ nm}$  [13]). This means that a substantial fraction of the probing light wave propagates along the interface where no affinity reaction took place.

In order to overcome this drawback for neutral or only weakly charged analyte molecules, the interfacial architecture that functionalizes the sensor surface for a specific affinity binding reaction was tailored as a brush or hydrogel matrix for which the extend of the evanescent field of the surface plasmon mode and the thickness of the binding matrix were matched [14]. The principle of this concept is shown in Figure 17.8: The carboxyl group of the brush polymer after activation by EDC/NHS chemistry can be used to bind to free amine groups of the protein that is used in the sensor design as the ligand to which the analyte from solution can bind specifically; in our example, a mouse IgG. Afterwards, any remaining free reactive ester groups not capped by a protein are passivated by reaction

Q2

Color Fig.: 17.7

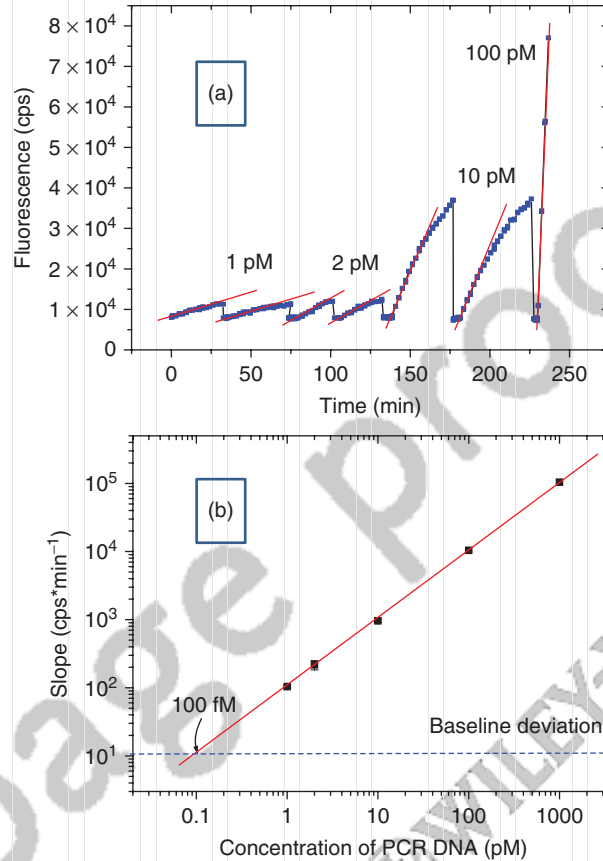


**Figure 17.7** LOD for a PCR amplicon demonstrated by monitoring (via SPFS) the (mass transfer limited) binding of the amplicons from solution to a PNA capture strand surface: (a) gives a series of time-dependent fluorescence curves obtained after injecting amplicon solutions of varying (extremely low) concentrations, running the binding reactions for a while, then rinsing pure buffer through the cell and regenerating the sensor

surface by an NaOH pulse before starting the next binding event. The red lines are linear fits to the early stage of the fluorescence increase by binding to the surface; (b) shows a plot of the slopes obtained from the binding curves in (a) as a function of bulk concentration. The intersection of the fit to this calibration curve (red line) with the baseline (background fluorescence level) results in an LOD of 100 fM.

with ethanolamine. The (IgG) protein concentration of the reaction solution during the functionalization and the reaction time are parameters that allow for a rather precise control of the degree of loading of the brush or hydrogel with the desired amount of binding sites. This makes this protocol rather simple and reliable. It should be noted, however, that nonactivated  $\text{COO}^-$  groups of the polymer matrix or active ester moieties that back-react by hydrolysis to free acid groups may lead to an undesired and rather uncontrolled background charge density in

Color Fig.: 17.8

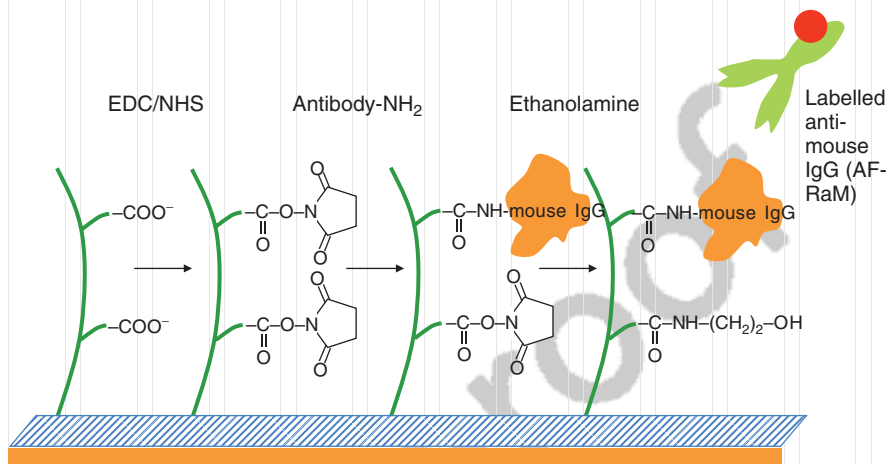


**Figure 17.8** Biofunctionalization of a brush on an optical transducer surface by an antibody: the carboxyl groups of the brush chains are activated by EDC/NHS chemistry, and then used to bind mouse antibodies to the brush. After passivation of any nonreacted active ester group by ethanolamine, the brush is ready for the binding of RaM-ABs that carry a chromophore label for SPFS detection.

the brush or the gel that may interfere with the loading of the sensor matrix by the binding site protein and/or with the affinity binding reaction with the analyte from solution.

In the system presented here, this analyte is a fluorophore-labeled rabbit anti-mouse antibody (cf. Figure 17.8), hence an example of a rather classical reaction scheme for an antibody–antigen recognition and binding event. The extreme sensitivity of the fluorescence detection by SPFS allows for monitoring binding processes at a bulk analyte concentration regime where no label-free detection scheme would ever allow for taking data: In the series of binding traces monitored in Figure 17.9, the bulk protein concentrations range from 16.7 fM to 333 aM ( $3 \times 10^{-16}$  M). Again, after each binding protocol at the different concentrations, a glycine buffer pulse regenerates the binding matrix in that it dissociates any bound antibody [15].

However, it can be seen in Figure 17.9 that for these extremely low concentrations, some proteins that may have denatured, hence cannot be detached by the glycine pulse anymore because they may sit within the matrix in a rather non-specifically physisorbed manner, however, still carry their fluorescent probe. This prevents the system – when regenerated – from reaching the background fluorescence seen in the absence of any chromophore-labeled proteins.

Still, the fluorescence increase monitored after the application of the analyte solution to the flow cell attached to the sensor chip can be fitted well by a straight line. The corresponding slope of this linear fluorescence increase as a function of time is highly bulk concentration dependent and results, when plotted again as a function of the corresponding bulk concentration (over a concentration range

Color Fig.: 17.9

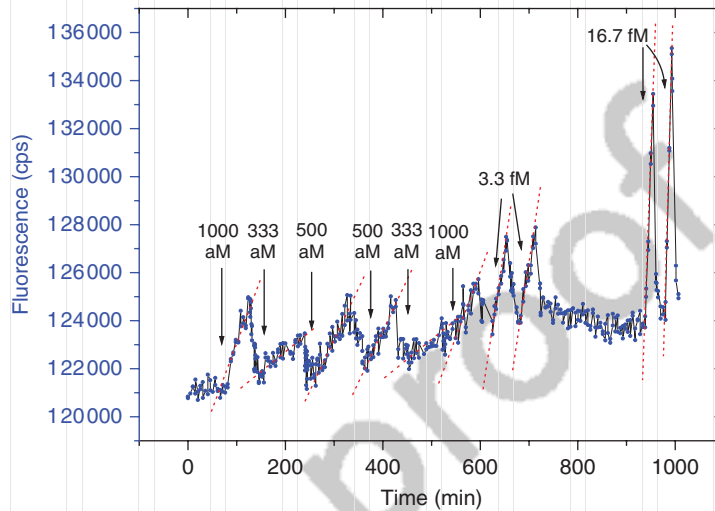


**Figure 17.9** Time-dependent fluorescence signal upon series of injections of rat-anti-mouse-antibody (RaM AB) solutions of varying (extremely low) concentrations, running the binding reactions for a while, then rinsing glycine buffer through the cell to

regenerating the sensor surface before starting the next binding event. The red dotted lines are linear fits to the fluorescence increase by binding of the RaMABs to the surface.

of six orders of magnitude, which means that the fluorescence increase for the highest concentrations is a million times faster than for the lowest concentration applied), in a calibration curve with an LOD = 500 aM (cf. Figure 17.10).

These binding curves can only be monitored label-free at much higher concentrations, starting roughly at nM concentrations one can calibrate the fluorescence increase seen at the extreme low concentration to the corresponding protein flux across the unstirred layer: at the level of the LOD, that is, 500 aM in our case, the observed fluorescence increase originates from 10 protein molecules per every  $\text{mm}^2$  on the sensor surface per every min. In other words, this technique is able to essentially record individual protein molecules that are approaching and binding to the sensor matrix.

#### 17.4

##### Monitoring Bacteria Binding to Functional Surfaces

The concept of matching the penetration depth of the evanescent field of a surface plasmon mode  $L_p$  to the distance from the sensor surface at which analyte binding occurs is demonstrated in another example. For instance, *E. coli* bacterial pathogens exhibit a size of few  $\mu\text{m}$  that is much larger than the decay length of the “normal” evanescent plasmon field. However, this decay length  $L_p$  can be engineered by introducing so-called long-range surface plasmon (LRSP) modes.

Color Fig.: 17.10

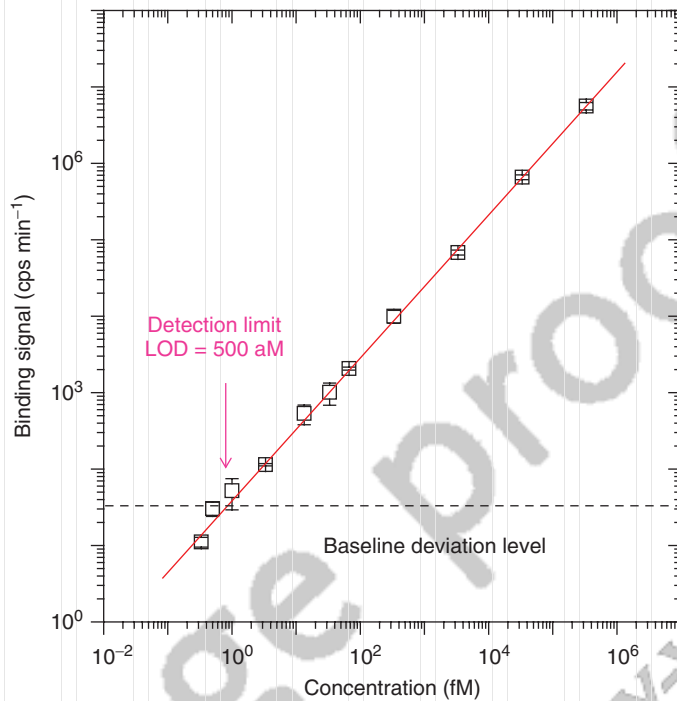


**Figure 17.10** Extremely sensitive biosensors by surface plasmon fluorescence spectroscopy (SPFS): shown is a plot of the slopes obtained from the binding curves in Figure 17.8 as a function of the

corresponding bulk concentration. The intersection of the fit to this calibration curve (red line) with the baseline (background fluorescence level) results in an LOD of 500 aM.

As is schematically demonstrated in Figure 17.11, the penetration depth of LRSPs field can be tuned to reach several micrometer and thus overlap with analytes as large as bacteria.

The occurrence of LRSPs and their use as excitation light source for fluorescence detection schemes in biosensing requires an interfacial architecture that allows for the coupling of two degenerate surface modes propagating along a thin metallic film [16, 17]. The interaction of surface plasmons with (nearly) identical dispersion behavior (i.e., energy–momentum relation) can be described as two coupled harmonic oscillators (the mechanical equivalent to this optical system is the coupled pendulum) and results in the establishing of two new eigenmodes. This phenomenon can be observed on metal layers with a thickness of several 10 nm sandwiched between two (nearly) identical dielectric media. Such geometry supports short-range surface plasmon (SRSP) and the LRSP modes. The latter is of particular interest to us here because it is highly de-damped. This means that a LRSP has a propagation length along the metal film much larger than a normal SP wave – a direct consequence of the much lower dissipation (damping) of its optical energy within the metal layer. Furthermore, its evanescent decay length  $L_p$

Color Fig.: 17.11

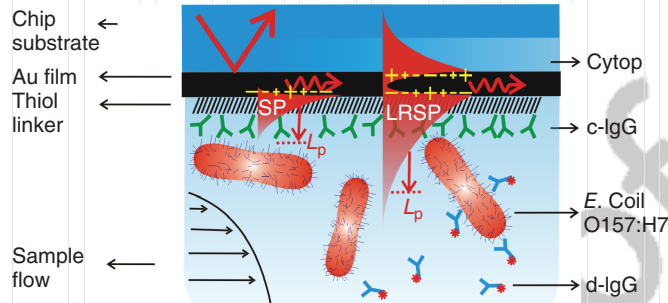


**Figure 17.11** Schematics of the layer architecture of a biosensor based on the excitation of long-range surface plasmon (LRSP) modes by the appropriate coupling of two degenerate surface plasmon modes. For details, see the text.

(perpendicular to the metal surface, i.e., the penetration depth into the dielectric medium) can be much larger than that of a normal surface plasmon: depending on parameters like the wavelength of the light, the optical characteristics of the metal and the dielectric material, and mostly on the thickness of the metal layer  $d_m$ . This decay length  $L_p$  can reach several micrometer in length and, hence, match nicely to effective the thickness of a layer of *E. coli* bacteria captured on this surface [18].

The experimental realization (Figure 17.11) of the excitation of coupled surface plasmons in water is not trivial because of the need for a symmetric dielectric environment with the given low dielectric constant of water. At first, this can be met by spin coating onto a glass substrate a thin (approx.  $d_b = 600$  nm in thickness, Figure 17.11) Teflon-like polymer support (e.g., Cytop, with a refractive index  $n = 1.34$ ) followed by a deposition of a thin SPR-active metal film. When brought in contact with an aqueous sample, this results in an experimental configuration where SRSP and LRSP modes can be excited in a classical Kretschmann setup (see Figure 17.4) [18].

For the detection of a specific strain of bacteria, that is, in our case *E. coli* O157:H7 which is a widely spread food-borne pathogen with an infective dose as low as 50–100 cells, the thin metal layer ( $d_m = 15.2$  nm) was first functionalized by a monolayer of a thiol derivative. The thiol SAM allows for the covalent chemical coupling of a capture antibody, c-IgG (cf. Figure 17.10), that specifically recognizes and binds this *E. coli* strain (that was, however, heat-killed for our studies). In the experiments, briefly reported here, the analyte solution with a specific concentration of bacteria, ranging from  $10^1$  to  $10^6$  colony forming units (cfu's) per ml, was circulating for 20 min through a flow cell, followed by rinsing the cell with pure buffer for 5 min, then incubating the sensor surface with a solution of the fluorescently labeled detection antibody d-IgG for 10 min and finally by another rinsing step with a buffer for 5 min. The protocol of such a series of experiments is given in Figure 17.12. Shown is the fluorescence intensity as a function of time originating from the d-IgG binding to the *E. coli* analyte. The black symbols and curves are obtained with the *E. coli* O157:H7 sample solutions;

Color Fig.: 17.12

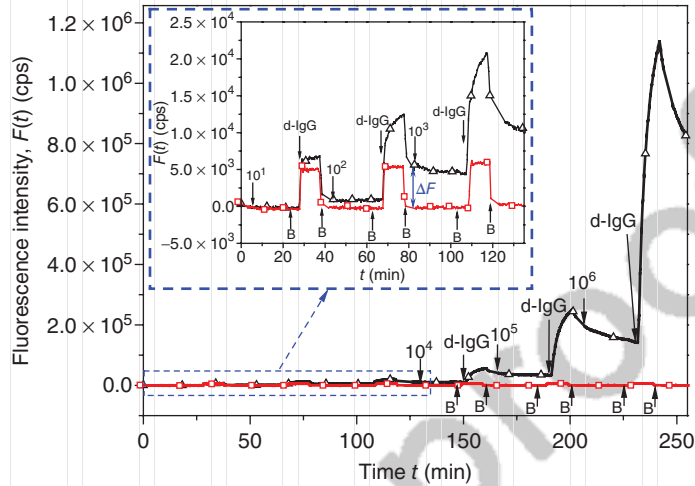


**Figure 17.12** Experimental protocol for the detection of bacteria by a sensor based on the excitation of long-range surface plasmon modes: analyte solution with a specific concentration of bacteria, ranging from  $10^1$  to  $10^6$   $\text{cfu ml}^{-1}$  (as indicated by the black arrows), was circulating for 20 min through the sample cell, followed by rinsing the cell with pure buffer for 5 min (indicated by the

black "B"), then incubating the sensor surface with the bound bacteria with a solution of the fluorescently labeled detection antibody d-IgG for 10 min, followed finally by another rinsing step with pure buffer for 5 min. The inset is a magnification of the fluorescence traces obtained for the lower bacterial concentrations. The red symbols were obtained with the reference *E. coli* K12 strain.

the red symbols and curves represent a series of control experiments with *E. coli* K12 cells. The inset is a magnification of the fluorescence traces obtained for the lower bacterial concentrations.

By plotting the fluorescence intensity,  $\Delta F$  (cf. the blue arrow in the inset of Figure 17.12), as a function of the applied bacterial concentration, one obtains again a calibration curve that intersects the background reference line given as a  $3\sigma(F)$  confidence level, at an  $\text{LOD} = 6 \text{ cfu ml}^{-1}$ , significantly lower than the infective dose (see Figure 17.13). This very high sensitivity is a direct result of matching the decay length of the probing field, a LRSP mode, to the size of the analyte, a bacterium. This way the whole bound *E. coli* is "seen" by the evanescent field and not only the slice of the first 150 nm closest to the interface as it would have been in the case of a normal SPR mode.

## 17.5 The t-BLM: A Novel Model Membrane Platform

To the various model membrane systems developed over the years – the Langmuir monolayers, uni- and multilamellar vesicles, the bimolecular ("black") lipid membrane – a novel configuration was recently added, called the t-BLM [8, 19].

Color Fig.: 17.13

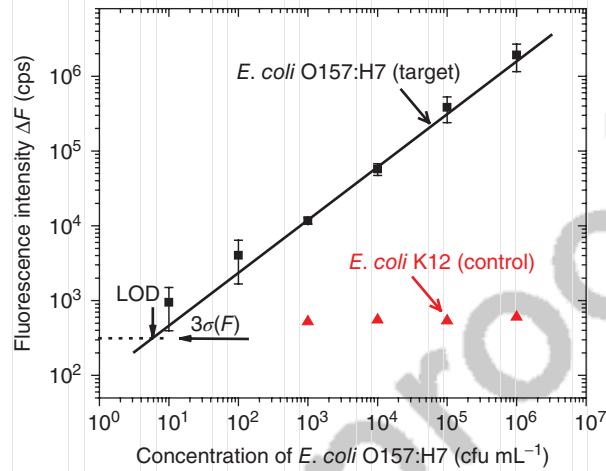


**Figure 17.13** Calibration curve for the detection of *E. coli* bacteria bound to the sensor surface via immobilized capture antibodies from bulk solutions of different bacterial concentrations. Plotted are the obtained fluorescence intensities ( $\Delta F$ , cf. Figure 17.11) as a function of the bulk bacterial concentration (in units of colony forming units per ml, cfu ml<sup>-1</sup>). The red data points are the reference measurement with *E. coli* K12, which are not recognized by the applied antibody.

This is considered to become a novel platform for biophysical studies of and with artificial membranes or for sensor development employing, for example, membrane-integral receptor proteins. Chemical coupling schemes based on thiol groups for Au substrates or silanes used in the case of oxide surfaces allow for the covalent and, hence, chemically and mechanically robust attachment of anchor lipids to the solid support, stabilizing the proximal layer of a tethered membrane on the transducer surface. This is schematically demonstrated in Figure 17.14 for the case of a Au substrate and thiol-based coupling chemistry: Onto the clean (and, hence, hydrophilic) Au substrate (used for surface plasmon optics and/or as the working electrode in electrochemical studies) (Figure 17.14a), a tethered monolayer is deposited by a self-assembly process of thiolated lipid derivatives from (typically an organic) solution (Figure 17.14b). When brought into contact with a lipid vesicle solution, the high surface energy of the alkane (methyl endgroup)/water interface represents a strong driving force for the fusion (wetting) of the vesicles onto the tethered monolayer, resulting in the desired architectures, that is, the tethered bimolecular lipid bilayer membrane (Figure 17.14c). When using (membrane) protein-functionalized vesicles for the final fusion step, these proteins then are transferred together with the vesicles and functionalize the tethered membrane by this desired protein structure, typically receptor systems, channel proteins, redox proteins, and others (Figure 17.14d).

Surface plasmon optics; the quartz crystal microbalance; fluorescence, Raman, and IR spectroscopies; scanning probe microscopies; and electrochemical techniques (including impedance spectroscopy) are typically used to characterize the buildup and the structural and functional properties of these complex

Color Fig.: 17.14

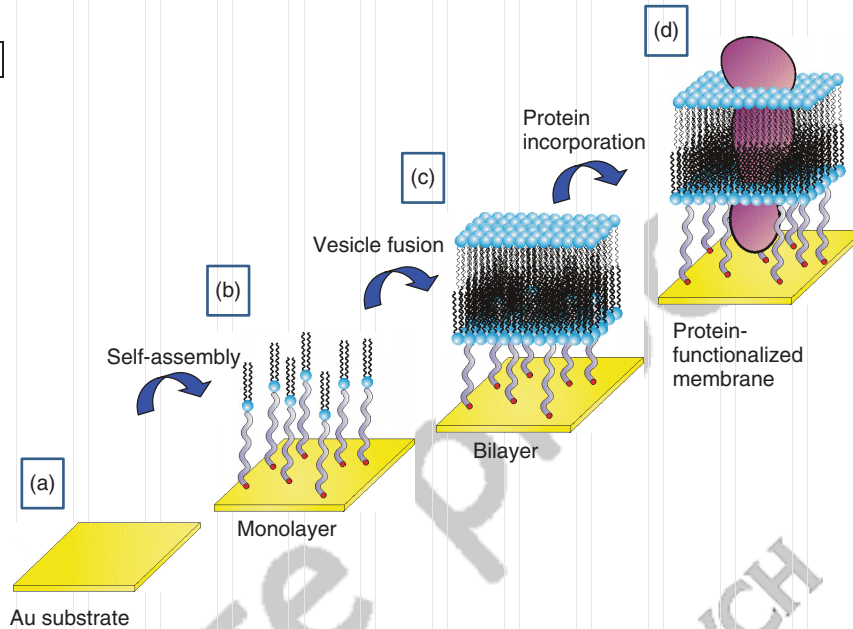


**Figure 17.14** Schematics of the buildup of a tethered bimolecular lipid membrane by a self-assembly process: on the clean Au substrate (a), a tethered monolayer is formed by the self-assembly of lipid derivatives, carrying, for example, a thiol or lipoic acid head group, the sulfur atoms of which interact strongly with the Au atoms of the substrate, thus overcompensating the loss of entropy by the ordering of the lipid chains upon forming the monolayer by the gain in

enthalpic energy (b). By exposing the methyl endgroups of the tethered monolayer in the aqueous environment of a lipid vesicle dispersion, the desired architecture, that is, a tethered lipid bilayer membrane, is spontaneously formed by the fusion of individual vesicles to the tethered monolayer (c). When vesicles with incorporated membrane proteins are used in this fusion step, a functionalized tethered bimolecular lipid membrane is obtained (d).

supramolecular interfacial architectures. In the absence of any channel protein or synthetic ionophore, lipid bilayers with a specific electrical resistance of better than  $10 \text{ M}\Omega \text{ cm}^2$  can be achieved routinely with this approach. Such a low conductance value (e.g., an electrode of  $100 \times 100 \mu\text{m}^2$  covered by such a tethered membrane has a background resistance of  $R = 10^{10} \Omega$ , hence represents a gigaseal situation known from patch clamping. This allows then for single-channel experiments as demonstrated in Figure 17.15 [20]: (a) shows thematically the interfacial architecture of a future membrane chip – an array of membrane patches, each functionalized by a specific pore or channel system, for example, for the high-throughput screening of a library of receptor proteins and (b) shows the experimental realization as it was demonstrated recently by our group: the microelectrodes of  $100 \times 100 \mu\text{m}^2$  are covered by a t-BLM, functionalized with a few channel proteins (the inner pore structure, M2, of the acetylcholine receptor (AChR)), covered by a drop of electrolyte solution to which a patch clamp

Color Fig.: 17.15

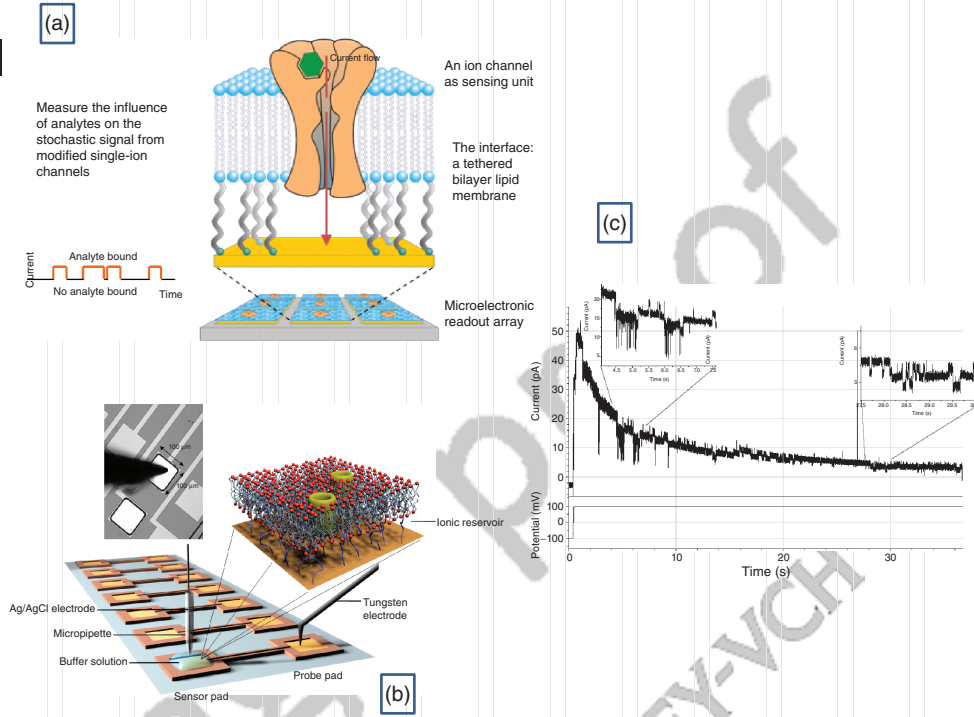


**Figure 17.15** (a) Schematics of a membrane chip. That is, an array of tBLM-covered microelectrodes, each functionalized with an individual channel protein, allowing for the recording of the stochastic opening and closing of each of these channels separately. (b) Details of the electrical readout by a patch clamp amplifier; the photograph shows an individual microelectrode,  $100 \times 100 \mu\text{m}^2$  in size, with the amplifier tip touching the electrolyte drop that sits on top of the tBLM-covered electrode. (c) Recording of

the electrical current, though such an individual membrane patch after applying a voltage jump from 0 to 100 mV: superimposed on the current decay (caused by the non-specific redistribution of the ions on both sides of the membrane upon changing the voltage across the membrane resulting in a counter-potential that develops by the ion asymmetry), one can clearly see the fluctuating current contribution originating from the opening and closing of individual channels in the membrane patch.

electrode is coupled. The working microelectrode is connected to the amplifier via a probe pad and a tungsten electrode.

Upon switching the voltage across the membrane (or more precisely between the Au substrate as the working electrode and the counter electrode in contact with the electrolyte solution on top of the membrane) from 0 to +100 mV (positive potential at the Au electrode), a current trace is observed as documented in Figure 17.15(c): the electrical current decays from an initial value of several 10 pA over a time period of several 10 min to a new stationary value of a few pA only. Dynamic simulations of this electrical circuit taking into account the passive permeation of  $\text{K}^+$  ions across the bilayer membrane (under the influence of

Druckfreigabe/approval for printing	
Without corrections/ ohne Korrekturen	<input type="checkbox"/>
After corrections/ nach Ausführung der Korrekturen	<input type="checkbox"/>
Date/Datum:	.....
Signature/Zeichen:	.....

the applied voltage) confirmed that this is the result of the depletion of potassium ions (from 100 to 85 mM in our case) in the thin cleft (a few nanometer only) between the bilayer and the electrode surface, defined by the length of the tether, and the concomitant counter voltage that builds up by the resulting ion asymmetry, leading to a reduced effective voltage across the lipid bilayer and hence a reduced driving force for the current.

Superimposed on this decay, one finds current fluctuations that result from the stochastic opening and closing of individual channel proteins reconstituted into the tethered lipid membrane that covers the microelectrode patch. The detailed analysis of the individual current increment for each opening event results in a unit current value of  $\Delta I = 0.7$  pA.

This very particular biofunctional interface opens a whole new area for biosensors that addresses the physiology of membrane proteins, for example, simple channels receptors, GPCRs, and so on. Considering that more than 60% of all drugs currently developed are targeting membrane-bound proteins, the introduction of this stable and robust sensor platform promises to have an enormous impact in the field of membrane biophysics and sensor development.

## 17.6 Conclusions

Biofunctional interfaces, that is, synthetic interfacial architectures that allow for the design of surfaces that are not only tolerated by body liquids, cells, tissue, or whole organisms, rather allow for the construction of interactive biointerfaces that allow for communication between the living world and the technical device, have reached a wide variety of maturity depending on (i) the chemical nature of the molecular assemblies that are immobilized on the surface, (ii) the complexity of the interfacial architecture, and (iii) the type of application they are designed for, ranging from disposable sensor chips to medical implants. Correspondingly, also the time span of use they are designed for range from minutes during which a measurement is done to many years as the expected time period for an implant staying in the human body.

Focusing on biofunctional surfaces for chip technologies, as we have done here in this chapter, we can state that the gene chip is the most advanced: it is on the market, is in frequent demand and use, and can be considered to be at a technical readiness level that requires only residual fine-tuning efforts for its functional performance.

This looks already rather different for the much needed protein chip: although offered commercially in a variety of formats, it is far from being completely under control. There are still many fundamental questions that remain to be answered: there is the basic challenge of the mere surface immobilization of functional proteins to the surface of a solid substrate in terms of structure, organization, dynamics, and, related to all that, the functional performance of a protein array. The

Druckfreigabe/approval for printing	
Without corrections/ ohne Korrekturen	<input type="checkbox"/> Trim Size: 170mm x 244mm
After corrections/ nach Ausführung der Korrekturen	<input type="checkbox"/>
Date/Datum:	.....
Signature/Zeichen:	.....

lifetime of the chip, both in terms of shelf life and during use, is a serious complication for the wider spread and use of protein chip technologies, in particular, when it comes to validation and certification of the measured data, for example, biomarker binding affinities.

The membrane chip as the most complex interfacial architecture described here is in a very early exploratory stage; it is a research topic that offers an enormous potential that is related to many aspects of medical and biotechnical applications: the search for new antimicrobial peptides as novel antibiotics that might get us out of the dilemma with multi-resistant bacterial strains, superbugs, that are among the most frightening problems in future clinical health care units, the search for drugs targeting the many membrane-integral receptors, and functional proteins like channels and pores, for which we have no high-throughput screening platform, to the design of completely novel sensor chips, for example, as artificial nose, or for the (technical) monitoring of taste in food technology. For the membrane chip, the options for technical applications are wide open but require in a particular way the close translational interaction between different disciplines: from the clinic to the bench of the materials chemists, from the farm to the food engineers and from the environment to the biotechnologist. Much has been achieved, but exciting developments are yet to be seen in the future.

#### Acknowledgments

It is our particular pleasure to acknowledge the contribution of many colleagues to the material presented in this chapter. In particular, the work of Drs Randy Duran, Ingo Köper, Renate Naumann, Peter Nielsen, Heyoung Park, Stefan Schiller, Yi Wang, Danfeng Yao, and Fang Yu is gratefully acknowledged.

#### References

1. Knoll, W. (ed) (2013) *Handbook of Biofunctional Surfaces*, Pan Stanford Publishing, Singapore.
2. Ratner, B.D. and Bryant, S.J. (2004) Biomaterials: where we have been and where we are going. *Annu. Rev. Biomed. Eng.*, **6** (1), 41–75.
3. Huang, N., Vörös, J., De Paul, S.M., Textor, M., and Spencer, N.D. (2002) Biotin-derivatized poly(l-lysine)-g-poly(ethylene glycol): a novel polymeric interface for bioaffinity sensing. *Langmuir*, **18** (1), 220–230.
4. Yao, D., Kim, J., Nielsen, P., Sinner, E., and Knoll, W. (2005) Surface density dependence of PCR amplicon hybridization on PNA/DNA probe layers. *Biophys. J.*, **88** (4), 2745–2751.
5. Kingsmore, S.F. (2006) Multiplexed protein measurement: technologies and applications of protein and antibody arrays. *Nat. Rev. Drug Discovery*, **5** (4), 310–320.
6. Tanaka, M. and Sackmann, E. (2005) Polymer-supported membranes as models of the cell surface. *Nature*, **437** (7059), 656–663.
7. Naumann, R., Jonczyk, A., Kopp, A., van Esch, J., Ringsdorf, H., Knoll, W., and Gräber, P. (1995) Incorporation of membrane proteins in solid-supported

Druckfreigabe/approval for printing	
Without corrections/ ohne Korrekturen	<input type="checkbox"/>
After corrections/ nach Ausführung der Korrekturen	<input type="checkbox"/>
Date/Datum:	.....
Signature/Zeichen:	.....

- lipid layers. *Angew. Chem. Int. Ed.*, **34** (18), 2056–2058.
8. Knoll, W., Köper, I., Naumann, R.L.C., and Sinner, E. (2008) Tethered bimolecular lipid membranes - a novel model membrane platform. *Electrochim. Acta*, **53** (23), 6680–6689.
  9. Song, H., Ritz, S., Knoll, W., and Sinner, E.K. (2009) Conformation and topology of amyloid  $\beta$ -protein adsorbed on a tethered artificial membrane probed by surface plasmon field-enhanced fluorescence spectroscopy. *J. Struct. Biol.*, **168** (1), 117–124.
  10. Sinner, E.K., Ritz, S., Wang, Y., Dostalek, J., Jonas, U., and Knoll, W. (2010) Molecular controlled functional architectures. *Mater. Today*, **13** (4), 46–55.
  11. Yao, D., Yu, F., Kim, J., Scholz, J., Nielsen, P., Sinner, E.K., and Knoll, W. (2004) Surface plasmon field-enhanced fluorescence spectroscopy in PCR product analysis by peptide nucleic acid probes. *Nucl. Acids Res. J.*, **32** (22), 177–192.
  12. Park, H., Germini, A., Sforza, S., Corradini, R., Marchelli, R., and Knoll, W. (2006) Kinetic and affinity analyses of hybridization reactions between peptide nucleic acid probes and DNA targets using surface plasmon field-enhanced fluorescence spectroscopy. *Biointerphases*, **1** (4), 113–122.
  13. Knoll, W. (1998) Interfaces and thin films as seen by bound electromagnetic waves. *Annu. Rev. Phys. Chem.*, **49** (1), 569–638.
  14. Yu, F., Persson, B., Lofas, S., and Knoll, W. (2004) Surface plasmon fluorescence immunoassay of free prostate-specific antigen in human plasma at the femtomolar level. *Anal. Chem.*, **76** (22), 6765–6770.
  15. Yu, F., Persson, B., Lofas, S., and Knoll, W. (2004) Attomolar sensitivity in bioassays based on surface plasmon fluorescence spectroscopy. *J. Am. Chem. Soc.*, **126** (29), 8902–8903.
  16. Toma, K., Dostalek, J., and Knoll, W. (2011) Long range surface plasmon-coupled fluorescence emission for biosensor applications. *Opt. Express*, **19** (12), 11090–11099.
  17. Kasry, A. and Knoll, W. (2006) Long range surface plasmon fluorescence spectroscopy. *Appl. Phys. Lett.*, **89** (10), 101106.
  18. Huang, C.J., Dostalek, J., Sessitsch, A., and Knoll, W. (2011) Long-range surface plasmon-enhanced fluorescence spectroscopy biosensor for ultrasensitive detection of *E. coli* O157:H7. *Anal. Chem.*, **83** (3), 674–677.
  19. Knoll, W., Bender, K., Förch, R., Frank, C., Götz, H., Heibel, C., Jenkins, T., Jonas, U., Kibrom, A., Kugler, R., Naumann, C., Naumann, R., Reisinger, A., Rühle, J., Schiller, S., and Sinner, E.K. (2010) Polymer-tethered bimolecular lipid membranes. *Polym. Membr. Biomembr.*, **224**, 87–111.
  20. Keizer, H.M., Dorvel, B.R., Andersson, M., Fine, D., Price, R.B., Long, J.R., Dodabalapur, A., Köper, I., Knoll, W., Anderson, P.A., and Duran, R.S. (2007) Functional ion channels in tethered bilayer membranes - implications for biosensors. *ChemBioChem*, **8** (11), 1246–1250.

Druckfreigabe/approval for printing

---

Without corrections/  
ohne Korrekturen

---

After corrections/  
nach Ausführung  
der Korrekturen

---

Date/Datum: .....

Signature/Zeichen: .....

Trim Size: 170mm x 244mm

Page Proof

WILEY-VCH

Druckfreigabe/approval for printing	
Without corrections/ ohne Korrekturen	<input type="checkbox"/>
After corrections/ nach Ausführung der Korrekturen	<input type="checkbox"/>
Date/Datum:	.....
Signature/Zeichen:	.....

Trim Size: 170mm x 244mm

Fecht c17.tex V1 - 08/01/2014 11:33am Page 23

“keywords/abstract

Dear Author,

**Keywords and abstracts will normally not be included in the print version of your chapter but only in the online version (if not decided differently by Wiley-VCH).**

Thank you!”

Abstract

Keywords

Q4 **Affiliation for the Authors:** Wolfgang Knoll, Amal Kasry, and Jakub Dostalek  
AITAustrian Institute of Technology, [Donau-City-Straße 1, Wien, 1220, Austria](#)

Page proof  
WILEY-VCH

Druckfreigabe/approval for printing	
Without corrections/ ohne Korrekturen	<input type="checkbox"/>
After corrections/ nach Ausführung der Korrekturen	<input type="checkbox"/>
Date/Datum:	.....
Signature/Zeichen:	.....

Trim Size: 170mm x 244mm

Fecht c17.tex V1 - 08/01/2014 11:33am Page 23

### Queries in Chapter 17

- Q1. Kindly confirm if the shortened running head is correct.
- Q2. Please confirm if these abbreviations 'EDC/NHS, SP, GPCR and S/N.' need to be spelt out. If yes, please provide the expansions.
- Q3. Please check the sentence 'This decay length...' and consider rephrasing it for clarity.
- Q4. Please provide department name and university name for the affiliation.

Page Proof  
WILEY-VCH